ACS Catalysis

pubs.acs.org/acscatalysis

Research Article

Simultaneous Evaluation of Reaction and Diffusion over Molecular Sieves for Shape-Selective Catalysis

Jingfeng Han, Zhiqiang Liu, Hua Li, Jiawei Zhong, Wenna Zhang, Jindou Huang, Anmin Zheng, Yingxu Wei,* and Zhongmin Liu*

Cite This: *ACS Catal.* 2020, 10, 8727–8735

Read Online

ACCESS | Metrics & More | Article Recommendations | Supporting Information

ABSTRACT: Shape selectivity is the critical issue of molecular sieve catalysis. As an important aspect of shape-selective catalysis, the significance of diffusion in conversion, deactivation, and product selectivity over molecular sieve catalysts has been recognized but still has not been interpreted quantitatively and explicitly. In the present work, direct tracking molecular diffusion in the SAPO-34 catalyst during the methanol-to-olefins (MTO) reaction is successfully realized by combining the MTO reaction with the diffusivity evaluation by a pseudo-gas chromatography method which was operated in one catalyst bed under the real reaction condition. Diffusion behavior over the working catalyst can be measured along with the reaction to reflect the evolution in shape-selectivity catalysis in real time. For the first time, the accessibility of the catalyst microporous surface for the reactant was quantified during the reaction, which provided a rational understanding of the reaction and deactivation of MTO over the catalyst with continuous coke deposition. The evaluation of configurational diffusion hindrance in SAPO-34, because of the accumulation of organic species retained in the catalyst, corresponds well to the evolution of methanol conversion and product distribution and provides the scientific basis for manipulating the MTO reaction from the point of shape-selective catalysis.

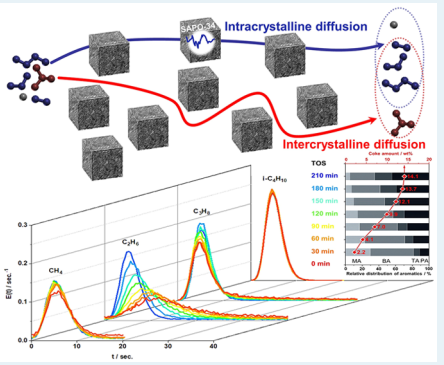

KEYWORDS: *methanol-to-olefins, reaction, diffusion, shape-selective catalysis, SAPO-34*

INTRODUCTION

Methanol-to-hydrocarbons (MTH) processes are the most successful route for the production of various and tuneable hydrocarbon products from C1 feedstock. One of the most challenging issues in MTH research is the control of product distribution, not only for the fundamental study related to the reaction mechanism but also for process industrialization. Distinct from the common acid-catalyzed reactions, a highly effective MTH process over acidic zeolite or zeotype catalysts follows the indirect reaction pathway for the hydrocarbon product formation with aromatic or alkenyl compounds as the reaction intermediates.[1] The product distribution of the MTH reaction highly depends on the reaction routes, which are closely related to the topology of the zeolite catalysts used.[2,3] For methanol conversion over ZSM-5, ethene and aromatics are predominantly produced through an aromatic-based reaction route, while propene and higher homologues are generated via the methylation-cracking pathway.[4] Following the olefin-based reaction route, propene and butene are the main products of MTH reaction over ZSM-22 and SAPO-11 with a 10-membered ring (10-MR) window.[5] As for SAPO-34 with an 8-membered ring (8-MR) window, light linear olefins are the main products and various aromatics and long chain olefins are trapped in the cavities, serving as reaction intermediates and/or inactive coke[6,7] (Scheme 1).

Scheme 1. Retained Species Generated from Methanol Conversion in SAPO-34 Causes the Diffusion Restriction for Reactant and Products

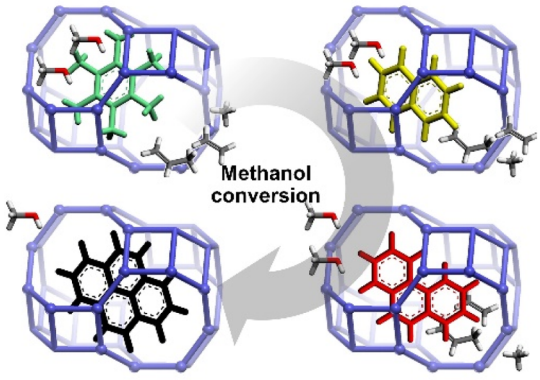

Received: May 8, 2020
Revised: July 1, 2020
Published: July 10, 2020

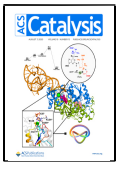

https://dx.doi.org/10.1021/acscatal.0c02054
ACS Catal. 2020, 10, 8727–8735

Based on the high selectivity toward light olefins, SAPO-34 is successfully applied as the catalyst in the industrialized methanol-to-olefins (MTO) technology in China.[6,8] During the MTO reaction over SAPO-34, the ethene selectivity increases as methanol feeding is prolonged, while the selectivity to other olefin homologues decreases.[9−11] The shift of product distribution to smaller hydrocarbons with time on stream could be ascribed to the change in the reaction routes of olefin generation with the involvement of confined organic species varying with time on stream[12−14] on one hand and the diffusion restriction resulting from the accumulation of confined coke species[15] on the other hand. Compared with the intensive study of the reaction mechanism and the reaction network of the MTO reaction, new techniques for diffusion measurements[16] were required to present the mass transfer of the reactant and products for the catalyst design.[17] The evolution of diffusion properties and its impact on catalytic performances, including the relationship between conversion and the accessibility of acid sites of the catalyst and the relationship between product selectivity and the difference in mass transfer of these products, have not been clearly revealed because of the difficulty in measuring and describing the diffusion properties of a variety of hydrocarbon products under the real reaction condition of MTO. Hence, in the present study, for the first time, MTO reaction evaluation combined with an online diffusivity measurement was performed simultaneously on one home-made equipment to determine the gradual variation of the diffusion property of molecules in SAPO-34 during the reaction and deactivation of methanol conversion. The accessibility of catalyst active sites with the reactant can be evaluated by the diffusion measurement with probe molecules and further correlated with the methanol conversion and catalyst deactivation quantitatively and rationally. At the same time, the selectivity evolution can also be explained from the point of product shape selectivity over the catalyst with coke deposition. Such knowledge has been highly required in the strategy proposal for the reaction and selectivity control of the MTO reaction catalyzed by the 8-MR and the cavity-type SAPO catalyst.

Herein, we performed a real-time investigation of the methanol reaction and the diffusion behavior in the SAPO-34 catalyst. Methanol conversion was conducted in a fixed bed reactor containing 60−80 mesh catalyst pellets. At various reaction stages of MTO, feeding the probe molecules of alkanes and evaluating their mass transfer in the catalyst bed allow us to present a complete prospect of reaction and diffusion in the MTO system with confined organic species in the catalyst. The residence time distribution (RTD) profiles of the probe molecules reveal the diffusivity variation of the reactant and products with the progress of the reaction and correspond well to the conversion, catalyst deactivation, and the evolution of product distribution.

EXPERIMENTAL SECTION

Catalyst Preparation. SAPO-34 (Si/(Si + Al + P) = 0.09) was synthesized by the method reported in the literature.[18] The corresponding characterization details of SAPO-34 have been described in the previous work.[19]

Ab Initio Molecular Dynamics Simulation for Pore Size Calculation of SAPO-34. It is well known that ab initio molecular dynamics (AIMD) simulation is a powerful tool to investigate the distributions of pore size.[20,21] In this work, AIMD simulation has been used to calculate the distribution of the pore size. The initial framework structure of pure silicon CHA was taken from the International Zeolite Association database,[22] and then the Si atoms in the CHA framework were substituted by Al and P atoms alternatively to form AlPO-34 zeolite and optimized by the CP2K code in the mixed Gaussian plane wave scheme.[23−25] To gain an insight into the effect of thermal expansion as well as into the flexibility on the lattice and the pore size of molecular sieves, the AIMD simulation was first performed in the *NPT* ensemble (constant number of particles *N*, pressure *P*, and temperature *T*) until the volume reached equilibrium at 1.0 bar. Then, a 30 ps AIMD simulation was performed in the canonical (*NVT*) ensemble. The simulated temperature was held at 373 K and controlled by the Nosé−Hoover thermostat.[26] The trajectories were recorded every step with a time step of 0.5 fs. Both the minimal and maximal pore size were counted from 5 to 30 ps after equilibration. During the simulation, the Perdew, Burke, and Ernzerhof exchange−correlation functional[27] was applied and the D3 correction[28] of Grimme was used to account for the dispersion interactions. The structures were relaxed by using the DZVP-MOLOPT-SR basis set and GTH pseudopotentials.[29] The plane wave cutoff energy and the relative cutoff energy were 650 and 60 Ry, respectively.

Combined MTO Reaction and Diffusion Evaluation. A combined catalytic reaction and diffusion evaluation system was self-developed in the lab and employed to conduct the MTO reaction and measure the diffusion property[30,31] alternately by switching methanol feeding for the reaction and pulsing the probe alkanes for diffusion evaluation (Scheme S1). With this system, a continuous flow methanol conversion was conducted over SAPO-34 at 500 °C with a space velocity of 2 h^{-1} until deactivation. A typical feeding procedure for the alternative reaction and diffusion evaluation system was as follows: (a) after helium purging, a pulse of 5% CH_4, 5% C_2H_6, and 5% C_3H_8 in helium gas was introduced onto the catalyst bed for diffusion measurements; (b) after the probe molecules fed in step (a) completely exited from the catalyst bed, 5% *i*-C_4H_{10} in helium gas was introduced onto the catalyst bed for 0.6 s for diffusion measurements; (c) methanol was fed for 30 min with a space velocity of 2 h^{-1} after diffusion measurements, and then the steps (a−c) were repeated. Before and after each step, the intensive purging of the catalyst bed with helium was conducted. Alkane diffusion probing and methanol reaction were recorded by online mass spectroscopy (MS) and gas chromatography (GC). Eight procedures of catalytic reaction and diffusion evaluation were operated until the SAPO-34 catalyst was completely deactivated, and then the spent catalyst was regenerated in air at 600 °C for 2 h. A comparative study of the continuous flow MTO reaction and the MTO reaction-alkane diffusion probing switch experiment was preformed, and no changes were observed on the catalytic properties of SAPO-34 (Figure S1).

Analysis of Retained Organics in SAPO-34. The retained organics in the catalysts after the MTO reaction for 500 °C for 2, 30, 60, 90, 120, 150, 180, and 210 min were analyzed by GC−MS. The catalysts were dissolved in 20% HF solution in a sealed Teflon vial, and the organic compounds were extracted with CH_2Cl_2 and analyzed by an Agilent 7890A-5975 GC−MS spectrometer equipped with an FID detector, a HP-5 capillary column (30 m × 0.25 mm×0.25 μm), and a mass selective detector. The structure identification is referenced to the NIST database. The amount of

https://dx.doi.org/10.1021/acscatal.0c02054
ACS Catal. 2020, 10, 8727−8735

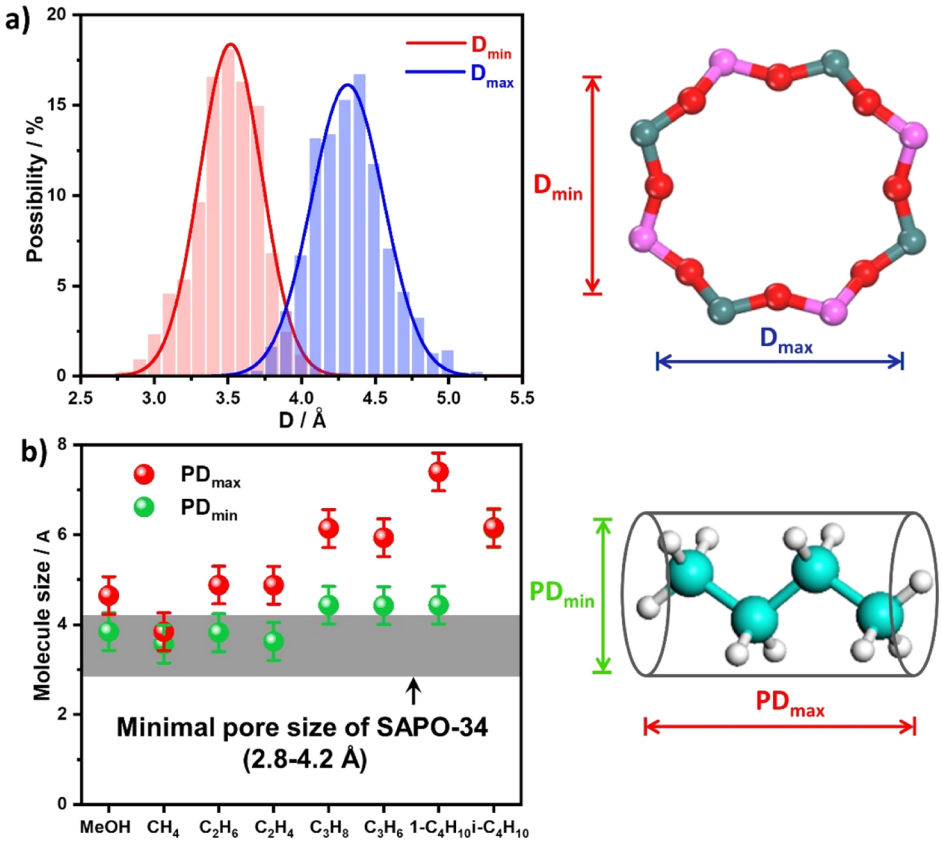

Figure 1. Calculation of the pore size of SAPO-34 with the AIMD method (a) and the minimal projection diameter (PD_{min}) and the maximal projection diameter (PD_{min}) of hydrocarbons compared with the pore size of SAPO-34 (b).

hydrocarbon compounds was determined using C_2Cl_6 as the internal standard.

Thermogravimetric analysis and differential thermogravimetry with SDT Q 600 were conducted to measure the coke removal. The catalysts after methanol reaction at 500 °C for 2, 30, 60, 90, 120, 150, 180, and 210 min were heated from room temperature to 900 °C at a rate of 10 °C/min under flowing air (100 mL/min). During the procedure, each sample was kept at 150 °C for 60 min for complete removal of adsorbed water.

RESULTS AND DISCUSSION

Projection Diameter of Probe Molecules. To discuss the diffusion-related shape selectivity of a molecular sieve-catalyzed reaction, the interference of strong adsorption of molecules onto the catalyst surface should be avoided in diffusion behavior evaluation. Therefore, in this paper, alkanes were used as probe molecules instead of alkenes and methanol to minimize the influence of adsorption and desorption. Methane, ethane, propane, and isobutane were selected as the probe molecules of the SAPO-34-catalyzed MTO reaction. The probe molecule was chosen considering their size and configuration. The size of SAPO-34 pore opening and probe hydrocarbons is theoretically predicted and compared in Figure 1.

The pore size of SAPO-34 was precisely calculated by the AIMD method.[20,21,26,27,29] Because of the effect of temperature and flexibility of the molecular sieve structure, the shape of the 8-ring window will be varied to a certain extent, which presents the minimal (D_{min}) and maximal (D_{max}) pore size as a function of time. It should be noted that D_{min} and D_{max} correspond to atoms that are not defined but will be changed and at the same time satisfy the relationship $D_{min} \leq D_{max}$; therefore, the distribution of pore size presents two peaks, as shown in Figure 1a. The feasibility of molecular diffusion in the molecular sieve crystal depends on the restriction of the pore opening on the guest molecules. Considering that most of the hydrocarbon products can be considered as spheroidal and cylindrical molecules, D_{min} in the range of 2.8−4.2 Å was used to evaluate the diffusion limitation on these guest molecules.

We used the minimal projection diameter (PD_{min}) and the maximal projection diameter (PD_{max}) to circumscribe the cylindrical[32,33] hydrocarbon molecules. PD_{min} and PD_{max} of the guest molecules were reckoned by the conformation of the molecular skeletons with the addition of a doubled hydrogen radius. The hydrogen radius would be overestimated if the van der Waals radius was adopted, which was used to calculate the pore size of SAPO-34 (1.35 Å for the O atom) because the C−H···O interaction between hydrocarbons and 8-MR of SAPO-34 was ignored. Thus, in this study, the hydrogen radius was estimated to be between 0.68 Å calibrated by the minimal length of the C−H···O hydrogen bond (2.08 Å)[34] and 1.1 Å (van der Waals radius of a H atom).

The calculated size of the hydrocarbon molecule and the D_{min} of 8-MR pore opening shown in Figure 1b can be used to estimate the feasibility of probe molecules passing through the 8-MR window of the SAPO-34 catalyst with intracrystalline diffusion. The calculated diameter of methane is smaller than the size of the 8-MR window. The PD_{min} and PD_{max} of ethane, which are close to that of methanol or ethene, are smaller or comparative to the 8-MR window. Therefore, the diffusion behavior of ethane with inert chemical properties can be used to represent the diffusion of methanol and ethene, which have

https://dx.doi.org/10.1021/acscatal.0c02054
ACS Catal. 2020, 10, 8727−8735

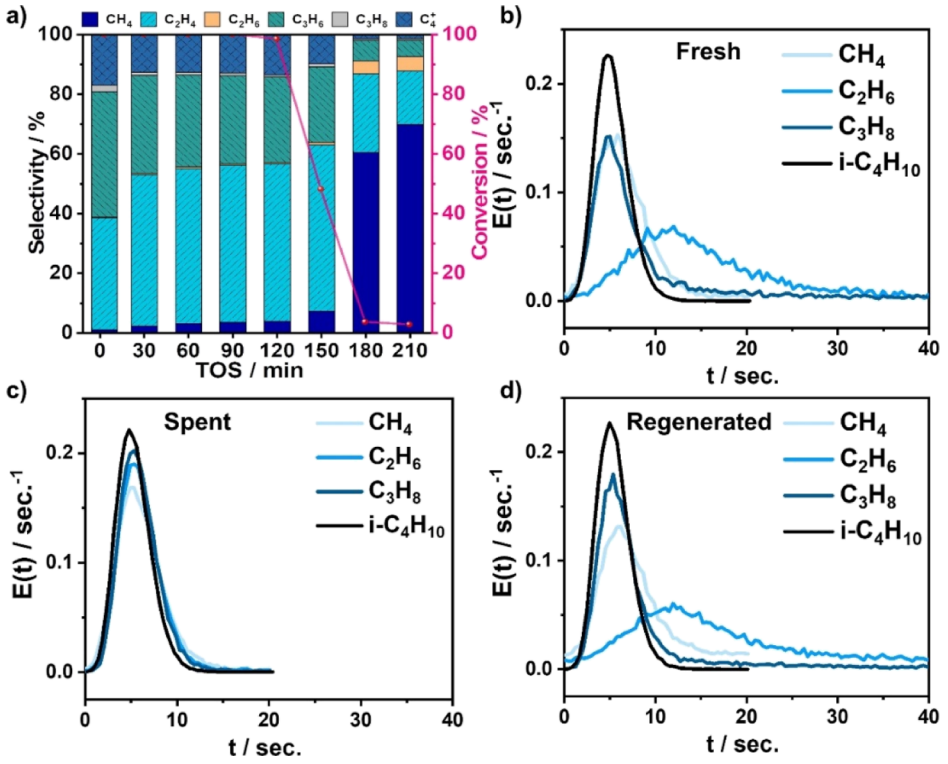

Figure 2. Methanol conversion and product distributions on SAPO-34 at 500 °C (a); $E(t)$-curves of probe molecule diffusion through the fresh (b), completely deactivated (c), and regenerated (d) catalyst bed.

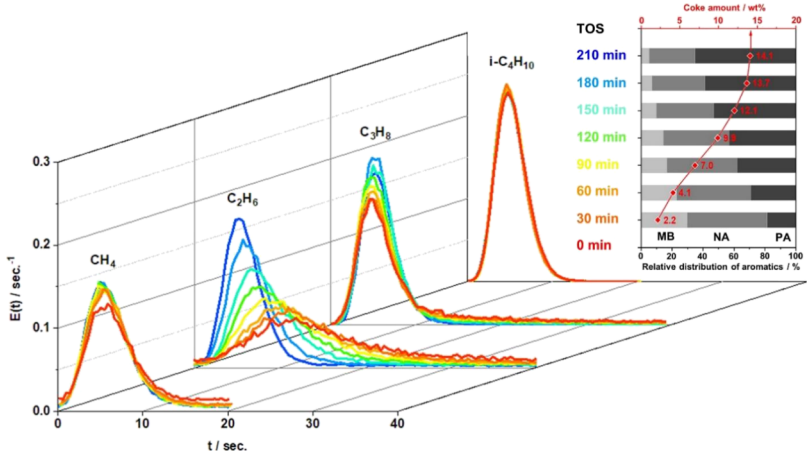

Figure 3. Experimental RTD curve ($E(t)$) of CH_4, C_2H_6, C_3H_8, and i-C_4H_{10} probing on the SAPO-34 catalyst bed during the MTO reaction. Inset: coke amount and distribution. MA, NA, and PA represent methyl-substituted benzenes, naphthalenes, and polyaromatics, respectively.

strong adsorption onto molecular sieve catalysts and are not suitable for diffusion evaluation. The PD_{min} of propane and propene is commensurate with the 8-MR window, while the PD_{max} is much higher. As compared in Figure 1b, the shape-selective diffusion of methanol, ethene, and propene in SAPO-34 could be speculated from that of ethane, ethane, and propane, respectively. The spherical isobutane molecule with a close PD_{min} and PD_{max} of over 5.7 Å was used as the probe molecule representing the hydrocarbon products with an even bulky size.

Diffusion Mode Determined from RTD of Probe Molecules. During the MTO reaction course, alkanes as probe molecules were injected onto the catalyst bed, and then, the concentration ($C(t)$) of the probe molecules escaping from the catalyst bed was detected using an online mass spectrometer. The RTD of the probe molecules passing through the catalyst bed, represented by $E(t)$, as a function of sweeping time t, is described by eq 1. Alkane diffusion in fresh, methanol-reacted, and regenerated catalyst beds were measured to testify the reliability of the method. The RTD profiles are plotted in Figure 2.

$$E(t) = \frac{C(t)}{\int_0^\infty C(t)\mathrm{d}t} \tag{1}$$

$E(t)$: function of RTD, t: probe molecule residence time in the catalyst bed, and $C(t)$: normalized portion of exited probe molecules from the catalyst bed, which is detected using a mass spectrometer at t.

https://dx.doi.org/10.1021/acscatal.0c02054
ACS Catal. 2020, 10, 8727−8735

Over the fresh SAPO-34 catalyst, the $E(t)$-curves of the probe alkanes indicate the various diffusion modes (Figure 2b). For methane and ethane, the $E(t)$-curves are presented as asymmetry peaks with a wide peak width and a relatively long residence time. Especially, ethane exiting from the catalyst bed requires a much longer time compared to methane. Comparatively, the propane and isobutane diffusion in the catalyst bed presented as the symmetry $E(t)$-curve with a short residence time. The $E(t)$-curves of propane show peak tailing to some extent (Figures 2b and 3). The $E(t)$-curve of isobutane presents the narrowest peak with a short residence time. Generally, for the probe molecule diffusion through the catalyst bed, the symmetry and narrow RTD peak with the shortest residence time indicates the intercrystalline diffusion mode; the widened and tailing peak with a relatively long RTD time, resulting from the interaction between the probe molecule and the catalyst, indicates that the molecule passes through the catalyst bed with intracrystalline diffusion but encounters the configurational diffusion restriction.[30,31] According to the observation in Figure 2, over the fresh SAPO-34 catalyst, methane and ethane go through the catalyst bed in the free intracrystalline diffusion mode; propane presents the intercrystalline diffusion mode for the majority and the intracrystalline diffusion mode for a small fraction due to the strong diffusion restriction; for isobutane, intracrystalline diffusion is impossible and the shortest residence time indicates the intercrystalline diffusion through the SAPO-34 catalyst bed.

The difference in the diffusion mode can also be interpreted according to the as-calculated project diameters of alkanes (Figure 1b). For methane and ethane with PD_{min} and PD_{max} lower than the pore size of SAPO-34, they can readily penetrate the crystal of SAPO-34 in the mode of intracrystalline diffusion. Even both methane and ethane can go through the catalyst bed by intracrystalline diffusion, and the broadened $E(t)$-curve of ethane implies that ethane encounters the enhanced intracrystalline diffusion hindrance compared with methane. As the pore size of SAPO-34 lies between the minimal and maximal projection diameters of propane, only a small portion of propane molecules could penetrate the crystals of SAPO-34 under the experimental conditions because of the severe configurational diffusion limitation, and most of the propane molecules pass through the catalyst bed in the intercrystalline diffusion mode. For isobutane with a PD_{min} over 5.7 Å, which is much larger than the pore size of SAPO-34, it goes through the catalyst bed only in the mode of intercrystalline diffusion, showing the narrowest RTD peak with the shorter residence time.

For the methanol-reacted catalyst, after reaction for 210 min (Figure 2a), with the occurrence of severe deactivation, the $E(t)$-curves for ethane and propane passing through the catalyst bed tend to be similar to that of isobutane, which indicates that the intracrystalline penetration is no longer feasible on the deactivated catalyst because of the mass-transfer reduction in the catalyst with coke deposition. The reduced intracrystalline diffusion indicates that not only the catalytic reaction center in microporous materials, to some extent, is no longer accessible for the reactant of methanol, but also the generated products inside SAPO-34 cannot escape from the catalysts. Comparatively, the very slight change in the $E(t)$-curve of CH_4 over fresh and deactivated catalysts shows that the cavity occupation with coke species has little influence on the diffusion of CH_4 with the smallest size, that is, CH_4 can still pass through the deactivated catalyst by the intracrystalline diffusion mode. This could also be confirmed by the predominant generation of methane at the TOS of 180 and 210 min in Figure 2a. After catalyst regeneration to remove the deposited coke, the $E(t)$-curves (Figure 2d) are identical to that over the fresh catalyst, indicating that the diffusion property of light alkanes in the SAPO-34 catalyst is completely recovered. In this way, the reliability of this diffusion evaluation method has also been confirmed.

Diffusion Evolution with Methanol Reaction over SAPO-34. To determine the mass-transfer evolution during methanol reaction over SAPO-34 with continuous coke deposition, the $E(t)$-curves of the probe alkane molecules were measured during the methanol reaction on SAPO-34 with a time interval of 30 min. The distribution and amount of retained species in SAPO-34 during methanol conversion at 500 °C are shown in Figure 3. When probing with CH_4, as the reaction time was prolonged, a series of $E(t)$-curves show a very slight change, as methane can diffuse freely in and out of the 8-MR window of SAPO-34, even with coke species located in the cavity of SAPO-34. Comparatively, the progress of the MTO reaction over SAPO-34 dramatically varies the diffusion of ethane in the catalyst bed. At the beginning of the reaction, the tailing peak in the $E(t)$-curve from ethane diffusion presents the typical intracrystalline diffusion character. With the progress of the reaction, the peak shifts to the shortened residence time range and becomes narrow in width, representing the increase in intercrystalline diffusion due to the increased difficulty in ethane mass transfer in the crystal catalyst with coke deposition. The tailing peak at a prolonged reaction time confirms that the intracrystalline diffusion is still feasible for ethane, although undergoing extremely strong restrictions. For propane probing, the peak location and symmetry of $E(t)$-curves show a very slight change with the reaction time and the build-up of the coke in the cavity structure of the catalyst. It is worth noting the predominant difference between ethane and propane diffusion. Compared to ethane, the very slight tailing of the propane peak from the beginning of the reaction indicates that the intracrystalline diffusion of propane, as a probe molecule, is more difficult than that of ethane even over the fresh catalyst. This result indicates that propane molecules passing through the catalyst bed via the intracrystalline diffusion mode are largely depressed over SAPO-34 compared to those of ethane. For the probe molecule of bulky i-C_4H_{10}, the diffusion through the catalyst bed gives only the symmetry and a narrow $E(t)$-curve without a tailing peak, as i-C_4H_{10} passes through the catalyst bed only via the intercrystalline diffusion mode. During the deactivation period, heavy coke deposition caused great diffusion restriction, thus intracrystalline diffusion was nearly completely prohibited for ethane and propane over the completely deactivated SAPO-34 catalyst. Intercrystalline diffusion became the only mode for the mass transfer of probe molecules, including ethane, propane, and i-C_4H_{10}. Mass transfer of the reactant and products is closely related to the catalytic activity and product generation. Measuring the varied diffusion property with the progress of the reaction can give a more complete and clearer understanding of the reaction and diffusion evolution caused by the coke deposition. As the obscure aspect of the reaction system in the past, diffusion cannot be considered well because of the lack of proper approach for precise detection and exact description.

https://dx.doi.org/10.1021/acscatal.0c02054
ACS Catal. 2020, 10, 8727−8735

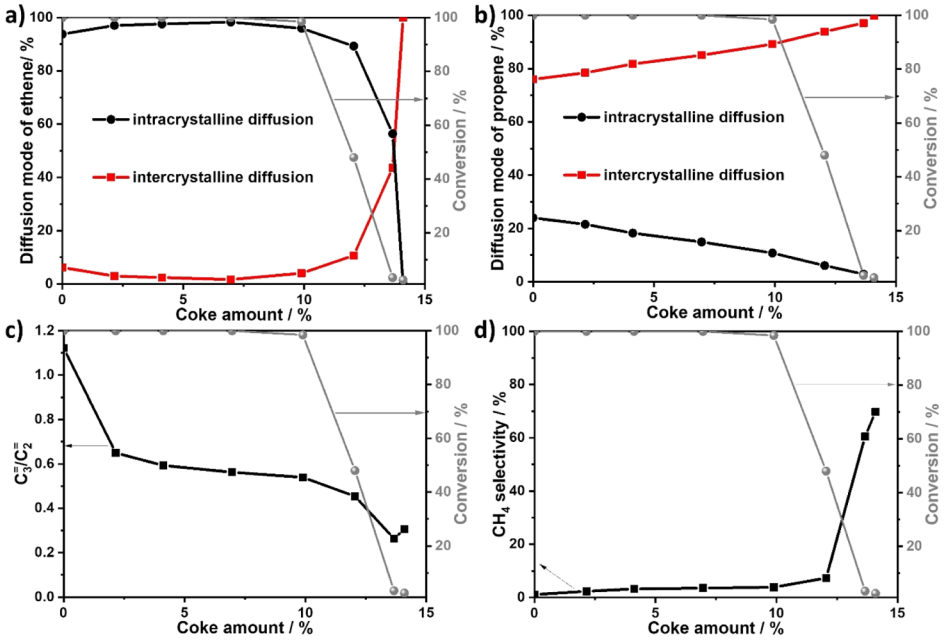

Figure 4. Variation of the diffusion mode of C_2H_6 (a) and C_3H_8 (b) and the ratio of propene selectivity to ethene selectivity (c) and CH_4 selectivity (d) with the increase of coke amount during methanol conversion.

According to the $E(t)$-curves, methane presents the sole intracrystalline diffusion behavior throughout the whole MTO reaction course, while *i*-C_4H_{10} only passes through the bed with the mode of intercrystalline mass transfer. For ethane and propane diffusion, their diffusion varies with the reaction time and coke deposition on SAPO-34. As the selected probe molecules are representative of the reactant and products, that is, the size of ethane is close to that of methanol or ethene, and the size of propane is close to that of propene based on the calculation results in Figure 1, determining the exact proportion of the diffusion mode of probe molecules, especially ethane and propane, will be of great significance for the rational interpretation of the reactant conversion and the selective production of light olefins during the reaction. With the simulation of $E(t)$-curves (Figures S2 and S3), for the first time, intercrystalline and intracrystalline diffusion can be separated by postulating that the $E(t)$-curves for ethane and propane diffusion over a completely deactivated catalyst (Figure 2c) represent the intercrystalline diffusion mode, and the detailed results are provided in Figure 4.

As shown in Figure 4a, for ethane diffusion, the proportion of intracrystalline diffusion accounts for 90% and remains nearly invariable before deactivation. While for propane, the percentage of intracrystalline diffusion mode is lower than 25% in the initial stage of MTO reaction and decreases gradually with time on stream (Figure 4b). The dominating diffusion mode for C_3H_8 is intercrystalline diffusion, consistent with the size of propane and the 8-MR in Figure 1b. The remarkable distinction of dominating the diffusion mode for ethane and propane indicates that the slight increment in the molecular size may lead to the change in the diffusion mode. Based on the diffusion evaluation with probe molecules, ethane and propane, during the MTO reaction, a much deeper insight into the reaction evolution including the conversion, the selective generation of olefin products, and the occurrence of secondary reactions can be elaborated reasonably based on combining the reaction understanding and mass-transfer evaluation together.

Correlating the Conversion and Product Generation with "Shape-Selective" Diffusion. Shape selectivity is an important feature and advantage of molecular sieve catalysis. When the probe molecules were used to study the molecular diffusion on the catalyst during methanol conversion, the change in the configurational diffusion was visually demonstrated by the reaction and the coke build-up in the SAPO-34 catalyst (Figure 3). The change in the diffusion properties of the probe molecules with coke deposition helps the rational understanding of the product shape selectivity and reactant shape selectivity in the reaction. In particular, by extracting intracrystalline and intercrystalline diffusion modes from the residence time curve, the diffusion evolution of the probe molecular ethane (having a projection diameter close to the reactant of methanol) is correlated with the reactant conversion on the microporous surface of the catalyst (Figure 4a). The quantification of the intracrystalline diffusion portion of the reactant reveals the accessibility of the reaction center for the reactant and gives a rational and quantitative understanding of the conversion and catalyst deactivation. The intracrystalline diffusion portion of methanol in the catalyst represents the effective contact of the reactant methanol with the microporous surface of the molecular sieve. The microporous surface accessibility of the catalyst for the reactant is completely consistent with the reaction conversion.

As can also be seen from Figure 4a, the speculated diffusion mode of methanol (probed by ethane) over SAPO-34 follows the intracrystalline diffusion during the highly efficient reaction stage and turns into intercrystalline diffusion when the coke amount attained 10% (in weight percent). Almost at the same time, the methanol conversion begins to decrease. These results indicated that the deactivation occurred when methanol could not diffuse into the cavity of SAPO-34 through the 8-MR window. Therefore, the reason for deactivation over SAPO-34 is the blocking of the contact of methanol with the active reaction center because of the reactant shape selectivity from the limitation of the 8-MR catalyst with coke deposition.

https://dx.doi.org/10.1021/acscatal.0c02054
ACS Catal. 2020, 10, 8727−8735

For methanol conversion to hydrocarbons over molecular sieve catalysts, the predominant production of the light olefins on the acidic site of catalysts results from the acidic catalysis for hydrocarbon generation from the C1 reactant of methanol, and the product distribution depends on the product shape selectivity from the catalyst with an 8-MR and a cavity structure. The narrow pore opening of SAPO-34 provides a strong limitation on the generated hydrocarbons to diffuse out of the 8-MR window as effluent products.[19,35] From the product distribution evolution of the MTO reaction over SAPO-34 at 500 °C given in Figure 2a and Table S1, the main products are ethene and propene in the efficient reaction period. With the progress of the reaction, the product distribution gradually inclines toward ethene and smaller species. In the deactivation stage, CH_4 production increases rapidly and the selectivity for small products (ethene, ethane, and methane) is over 80%. Considering the sizes of the 8-MR window of SAPO-34 and hydrocarbon products, the restriction from the 8-MR window of SAPO-34 blocks the effluence of long-chain hydrocarbons and aromatics and permits the outflow of ethene and propene. With the methanol conversion and coke deposition on the catalyst, the diffusion barrier increases with the accumulation of coke species, leading to the gradual increase in ethene selectivity and the corresponding decrease in the selectivity for larger hydrocarbons. This variation of diffusion properties with the progress of the methanol reaction led to the sharp decrease of $C_3^=/C_2^=$ with the occurrence of coke deposition (Figure 4c). Notably, in the deactivation stage, the diffusion limitation is too strong to merely allow the diffusion of methane out of the catalyst crystal, leading to the enhanced selectivity of methane, which could be regarded as the signal of severe deactivation (Figure 4d).

CONCLUSIONS

In this work, a self-developed reaction and diffusion device is established and used to study the shape-selective catalysis in the MTO reaction system. The molecular diffusion behavior in the SAPO-34 catalyst bed was determined under the working conditions, and the catalytic performances of MTO conversion over the same catalyst bed were evaluated simultaneously. RTD profiles achieved from diffusion measurements using the probe molecule present the different mass transport mode in the catalyst bed. For the diffusion of the reactant or hydrocarbon products, the molecules passing through the catalyst bed of SAPO-34 depend highly on their size and configuration and evolve throughout the whole reaction course. The successful extraction of the intracrystalline and intercrystalline diffusion modes in the catalyst bed from RTD profiles quantifies the reactant shape selectivity and product shape selectivity. The intracrystalline diffusion of the reactant inside the catalyst causes the reactant reaction center contact and reaction occurrence, while the accessibility decrease of the catalyst microporous surface for methanol causes the decline of methanol conversion, corresponding to the occurrence of deactivation. The progress of the MTO reaction gives rise to enhanced intracrystalline diffusion limitation for large hydrocarbon products, leading to the increase of light olefin selectivity. These understandings enrich and rationalize the knowledge of shape-selective diffusion and reaction of zeolite-catalyzed processes and provide the scientific basis for reaction modulation and optimization based on the perspective of a diffusion-controlled MTO process.

ASSOCIATED CONTENT

Supporting Information

The Supporting Information is available free of charge at https://pubs.acs.org/doi/10.1021/acscatal.0c02054.

Experimental setup for conducting the catalytic reaction and diffusion measurements; product distribution of MTO reaction over SAPO-34; a comparison of continuous-flow MTO reaction and MTO reaction with interval alkane pulsing for diffusion measurement; and splitting of E(t)-curves of C_2H_6 and C_3H_8 diffusion through the fresh and methanol-reacted catalyst bed after reaction for various time periods (PDF)

AUTHOR INFORMATION

Corresponding Authors

Yingxu Wei − *National Engineering Laboratory for Methanol to Olefins, State Energy Low Carbon Catalysis and Engineering R&D Center, Dalian National Laboratory for Clean Energy, iChEM (Collaborative Innovation Center of Chemistry for Energy Materials), Dalian Institute of Chemical Physics, Chinese Academy of Sciences, Dalian 116023, Liaoning, China*; Email: weiyx@dicp.ac.cn

Zhongmin Liu − *National Engineering Laboratory for Methanol to Olefins, State Energy Low Carbon Catalysis and Engineering R&D Center, Dalian National Laboratory for Clean Energy, iChEM (Collaborative Innovation Center of Chemistry for Energy Materials), Dalian Institute of Chemical Physics and State Key Laboratory of Catalysis, Dalian Institute of Chemical Physics, Chinese Academy of Sciences, Dalian 116023, Liaoning, China*; orcid.org/0000-0002-7999-2940; Email: liuzm@dicp.ac.cn

Authors

Jingfeng Han − *National Engineering Laboratory for Methanol to Olefins, State Energy Low Carbon Catalysis and Engineering R&D Center, Dalian National Laboratory for Clean Energy, iChEM (Collaborative Innovation Center of Chemistry for Energy Materials), Dalian Institute of Chemical Physics, Chinese Academy of Sciences, Dalian 116023, Liaoning, China*

Zhiqiang Liu − *State Key Laboratory of Magnetic Resonance and Atomic and Molecular Physics, National Center for Magnetic Resonance in Wuhan, Key Laboratory of Magnetic Resonance in Biological Systems, Wuhan Institute of Physics and Mathematics, Innovation Academy for Precision Measurement Science and Technology, Chinese Academy of Sciences, Wuhan 430071, P.R. China*; orcid.org/0000-0003-2872-0125

Hua Li − *National Engineering Laboratory for Methanol to Olefins, State Energy Low Carbon Catalysis and Engineering R&D Center, Dalian National Laboratory for Clean Energy, iChEM (Collaborative Innovation Center of Chemistry for Energy Materials), Dalian Institute of Chemical Physics, Chinese Academy of Sciences, Dalian 116023, Liaoning, China*

Jiawei Zhong − *National Engineering Laboratory for Methanol to Olefins, State Energy Low Carbon Catalysis and Engineering R&D Center, Dalian National Laboratory for Clean Energy, iChEM (Collaborative Innovation Center of Chemistry for Energy Materials), Dalian Institute of Chemical Physics, Chinese Academy of Sciences, Dalian 116023, Liaoning, China; University of Chinese Academy of Sciences, Beijing 100049, China*

Wenna Zhang − *National Engineering Laboratory for Methanol to Olefins, State Energy Low Carbon Catalysis and Engineering*

https://dx.doi.org/10.1021/acscatal.0c02054
ACS Catal. 2020, 10, 8727−8735

R&D Center, Dalian National Laboratory for Clean Energy, iChEM (Collaborative Innovation Center of Chemistry for Energy Materials), Dalian Institute of Chemical Physics, Chinese Academy of Sciences, Dalian 116023, Liaoning, China

Jindou Huang − *National Engineering Laboratory for Methanol to Olefins, State Energy Low Carbon Catalysis and Engineering R&D Center, Dalian National Laboratory for Clean Energy, iChEM (Collaborative Innovation Center of Chemistry for Energy Materials), Dalian Institute of Chemical Physics, Chinese Academy of Sciences, Dalian 116023, Liaoning, China*

Anmin Zheng − *State Key Laboratory of Magnetic Resonance and Atomic and Molecular Physics, National Center for Magnetic Resonance in Wuhan, Key Laboratory of Magnetic Resonance in Biological Systems, Wuhan Institute of Physics and Mathematics, Innovation Academy for Precision Measurement Science and Technology, Chinese Academy of Sciences, Wuhan 430071, P.R. China; School of Materials Science and Engineering, Zhengzhou University, Zhengzhou, Henan 450001, P.R. China;* orcid.org/0000-0001-7115-6510

Complete contact information is available at: https://pubs.acs.org/10.1021/acscatal.0c02054

Author Contributions

The manuscript was written through contributions of all authors. All authors have given approval to the final version of the manuscript.

Notes

The authors declare no competing financial interest.

■ ACKNOWLEDGMENTS

The authors are thankful for the financial support from the National Natural Science Foundation of China (nos. 21991092, 21991090, 21603223, 91745109, 21703239, 21902153, and 21972142), the Key Research Program of Frontier Sciences, CAS, Grant no. QYZDY-SSW-JSC024, the International Partnership Program of Chinese Academy of Sciences (121421KYSB20180007), and Dalian Institute of Chemical Physics, grant no. DICP I201926.

■ REFERENCES

(1) Haw, J. F.; Song, W.; Marcus, D. M.; Nicholas, J. B. The mechanism of methanol to hydrocarbon catalysis. *Acc. Chem. Res.* **2003**, *36*, 317−326.

(2) Olsbye, U.; Svelle, S.; Bjørgen, M.; Beato, P.; Janssens, T. V. W.; Joensen, F.; Bordiga, S.; Lillerud, K. P. Conversion of Methanol to Hydrocarbons: How Zeolite Cavity and Pore Size Controls Product Selectivity. *Angew. Chem., Int. Ed.* **2012**, *51*, 5810−5831.

(3) Xu, S.; Zhi, Y.; Han, J.; Zhang, W.; Wu, X.; Sun, T.; Wei, Y.; Liu, Z. Advances in Catalysis for Methanol-to-Olefins Conversion. *Adv. Catal.* **2017**, *61*, 37−122.

(4) Svelle, S.; Joensen, F.; Nerlov, J.; Olsbye, U.; Lillerud, K.-P.; Kolboe, S.; Bjørgen, M. Conversion of methanol into hydrocarbons over zeolite H-ZSM-5: Ethene formation is mechanistically separated from the formation of higher alkenes. *J. Am. Chem. Soc.* **2006**, *128*, 14770−14771.

(5) Wang, J.; Li, J.; Xu, S.; Zhi, Y.; Wei, Y.; He, Y.; Chen, J.; Zhang, M.; Wang, Q.; Zhang, W.; Wu, X.; Guo, X.; Liu, Z. Methanol to hydrocarbons reaction over HZSM-22 and SAPO-11: Effect of catalyst acid strength on reaction and deactivation mechanism. *Chin. J. Catal.* **2015**, *36*, 1392−1402.

(6) Liang, J.; Li, H.; Zhao, S.; Guo, W.; Wang, R.; Ying, M. Characteristics and Performance of Sapo-34 Catalyst for Methanol-to-Olefin Conversion. *Appl. Catal.* **1990**, *64*, 31−40.

(7) Haw, J. F.; Marcus, D. M. Well-defined (supra)molecular structures in zeolite methanol-to-olefin catalysis. *Top. Catal.* **2005**, *34*, 41−48.

(8) Tian, P.; Wei, Y.; Ye, M.; Liu, Z. Methanol to Olefins (MTO): From Fundamentals to Commercialization. *ACS Catal.* **2015**, *5*, 1922−1938.

(9) Chen, D.; Grønvold, A.; Moljord, K.; Holmen, A. Methanol conversion to light olefins over SAPO-34: Reaction network and deactivation kinetics. *Ind. Eng. Chem. Res.* **2007**, *46*, 4116−4123.

(10) Dahl, I. M.; Wendelbo, R.; Andersen, A.; Akporiaye, D.; Mostad, H.; Fuglerud, T. The effect of crystallite size on the activity and selectivity of the reaction of ethanol and 2-propanol over SAPO-34. *Microporous Mesoporous Mater.* **1999**, *29*, 159−171.

(11) Wei, Y.; Yuan, C.; Li, J.; Xu, S.; Zhou, Y.; Chen, J.; Wang, Q.; Xu, L.; Qi, Y.; Zhang, Q.; Liu, Z. Coke Formation and Carbon Atom Economy of Methanol-to-Olefins Reaction. *ChemSusChem* **2012**, *5*, 906−912.

(12) Song, W.; Fu, H.; Haw, J. F. Supramolecular origins of product selectivity for methanol-to-olefin catalysis on HSAPO-34. *J. Am. Chem. Soc.* **2001**, *123*, 4749−4754.

(13) Chen, D.; Moljord, K.; Holmen, A. A methanol to olefins review: Diffusion, coke formation and deactivation SAPO type catalysts. *Microporous Mesoporous Mater.* **2012**, *164*, 239−250.

(14) Hereijgers, B. P. C.; Bleken, F.; Nilsen, M. H.; Svelle, S.; Lillerud, K.-P.; Bjørgen, M.; Weckhuysen, B. M.; Olsbye, U. Product shape selectivity dominates the Methanol-to-Olefins (MTO) reaction over H-SAPO-34 catalysts. *J. Catal.* **2009**, *264*, 77−87.

(15) Chen, D.; Moljord, K.; Fuglerud, T.; Holmen, A. The effect of crystal size of SAPO-34 on the selectivity and deactivation of the MTO reaction. *Microporous Mesoporous Mater.* **1999**, *29*, 191−203.

(16) Peng, P.; Stosic, D.; Aitblal, A.; Vimont, A.; Bazin, P.; Liu, X.-M.; Yan, Z.-F.; Mintova, S.; Travert, A. Unraveling the Diffusion Properties of Zeolite-Based Multicomponent Catalyst by Combined Gravimetric Analysis and IR Spectroscopy (AGIR). *ACS Catal.* **2020**, *10*, 6822−6830.

(17) Jiao, Y.; Forster, L.; Xu, S.; Chen, H.; Han, J.; Liu, X.; Zhou, Y.; Liu, J.; Zhang, J.; Yu, J.; D'Agostino, C.; Fan, X. Creation of Al-Enriched Mesoporous ZSM-5 Nanoboxes with High Catalytic Activity: Converting Tetrahedral Extra-Framework Al into Framework Sites by Post Treatment. *Angew Chem. Int. Ed.* **2020**, DOI: 10.1002/anie.202002416.

(18) Chen, J.; Li, J.; Wei, Y.; Yuan, C.; Li, B.; Xu, S.; Zhou, Y.; Wang, J.; Zhang, M.; Liu, Z. Spatial confinement effects of cage-type SAPO molecular sieves on product distribution and coke formation in methanol-to-olefin reaction. *Catal. Commun.* **2014**, *46*, 36−40.

(19) Zhang, W.; Zhi, Y.; Huang, J.; Wu, X.; Zeng, S.; Xu, S.; Zheng, A.; Wei, Y.; Liu, Z. Methanol to Olefins Reaction Route Based on Methylcyclopentadienes as Critical Intermediates. *ACS Catal.* **2019**, *9*, 7373−7379.

(20) Bereciartua, P. J.; Cantín, Á.; Corma, A.; Jordá, J. L.; Palomino, M.; Rey, F.; Valencia, S.; Corcoran, E. W.; Kortunov, P.; Ravikovitch, P. I.; Burton, A.; Yoon, C.; Wang, Y.; Paur, C.; Guzman, J.; Bishop, A. R.; Casty, G. L. Control of zeolite framework flexibility and pore topology for separation of ethane and ethylene. *Science* **2017**, *358*, 1068−1071.

(21) Shi, H.; Migues, A. N.; Auerbach, S. M. Ab initio and classical simulations of the temperature dependence of zeolite pore sizes. *Green Chem.* **2014**, *16*, 875−884.

(22) Baerlocher, C., McCusker, L. B. *Database of Zeolite Structures*, http://www.iza-structure.org/databases/ (Accessed June 2016).

(23) Hutter, J.; Iannuzzi, M.; Schiffmann, F.; VandeVondele, J. CP2K: Atomistic Simulations of Condensed Matter Systems. *J. Wires. Comput. Mol. Sci.* **2014**, *4*, 15−25.

(24) VandeVondele, J.; Krack, M.; Mohamed, F.; Parrinello, M.; Chassaing, T.; Hutter, J. QUICKSTEP: Fast and accurate density functional calculations using a mixed Gaussian and plane waves approach. *Comput. Phys. Commun.* **2005**, *167*, 103−128.

(25) VandeVondele, J.; Hutter, J. Gaussian basis sets for accurate calculations on molecular systems in gas and condensed phases. *J. Chem. Phys.* **2007**, *127*, 114105.
(26) Tuckerman, M. E.; Liu, Y.; Ciccotti, G.; Martyna, G. J. Non-Hamiltonian molecular dynamics: Generalizing Hamiltonian phase space principles to non-Hamiltonian systems. *J. Chem. Phys.* **2001**, *115*, 1678−1702.
(27) Perdew, J. P.; Burke, K.; Ernzerhof, M. Generalized gradient approximation made simple. *Phys. Rev. Lett.* **1997**, *78*, 1396.
(28) Grimme, S.; Antony, J.; Ehrlich, S.; Krieg, H. A consistent and accurate ab initio parametrization of density functional dispersion correction (DFT-D) for the 94 elements H-Pu. *J. Chem. Phys.* **2010**, *132*, 154104.
(29) Goedecker, S.; Teter, M.; Hutter, J. Separable dual-space Gaussian pseudopotentials. *Phys. Rev. B: Condens. Matter Mater. Phys.* **1996**, *54*, 1703−1710.
(30) Haynes, H. W.; Sarma, P. N. Model for Application of Gas-Chromatography to Measurements of Diffusion in Bidisperse Structured Catalysts. *AIChE J.* **1973**, *19*, 1043−1046.
(31) Arma, P. N. S.; Haynes, H. W.; Haynes, H. W. Application of Gas-Chromatography to Measurements of Diffusion in Zeolites. *Adv. Chem.* **1974**, *133*, 205−217.
(32) Petitjean, M. About the algebraic solutions of smallest enclosing cylinders problems. *Appl. Algebr. Eng. Comm.* **2012**, *23*, 151−164.
(33) Brandenberg, R.; Theobald, T. Algebraic methods for computing smallest enclosing and circumscribing cylinders of simplices. *Appl. Algebr. Eng. Comm.* **2004**, *14*, 439−460.
(34) Takusagawa, F.; Koetzle, T. F.; Srikrishnan, T.; Parthasarathy, R. C-H...O Interactions and Stacking of Water-Molecules between Pyrimidine-Bases in 5-Nitro-1-(Beta-D-Ribosyluronic Acid)-Uracil Monohydrate [1-(5-Nitro-2,4-Dioxopyrimidinyl)-Beta-D-Ribofuranoic Acid Monohydrate] - Neutron-Diffraction Study at 80 K. *Acta Crystallogr., Sect. B: Struct. Crystallogr. Cryst. Chem.* **1979**, *35*, 1388−1394.
(35) Li, J.; Wei, Y.; Chen, J.; Xu, S.; Tian, P.; Yang, X.; Li, B.; Wang, J.; Liu, Z. Cavity Controls the Selectivity: Insights of Confinement Effects on MTO Reaction. *ACS Catal.* **2015**, *5*, 661−665.

https://dx.doi.org/10.1021/acscatal.0c02054
ACS Catal. 2020, 10, 8727−8735